Role of *Fzd6* in Regulating the Osteogenic Differentiation of Adipose-derived Stem Cells in Osteoporosis

Tianli Wu
Southwest Medical University
Zhihao Yao
Southwest Medical University
Gang Tao
Southwest Medical University
Fangzhi Lou
Southwest Medical University
Hui Tang
Southwest Medical University
Yujin Gao
Southwest Medical University
Xiaojuan Yang
Tongji University
Jingang Xiao (drxiaojingang@163.com)
Southwest Medical University https://orcid.org/0000-0003-1548-2084

Research Article

Keywords: Osteoporosis, Adipose stem cells, Lentivirus, Fzd6, Osteogenic differentiation

Posted Date: March 22nd, 2021

DOI: https://doi.org/10.21203/rs.3.rs-328417/v1

Abstract

Objective: Although it has been demonstrated that adipose-derived stem cells (ASCs) from osteoporosis mice (OP-ASCs) exhibit impaired osteogenic differentiation potential, the molecular mechanism has not yet been elucidated. We found that *Fzd6* was decreased in OP-ASCs compared with ASCs. This study investigates the effects and underlying mechanisms of *Fzd6* in the osteogenic potential of OP-ASCs.

Methods: *Fzd6* expression in ASCs and OP-ASCs was measured by PCR gene chip. *Fzd6* overexpression and silencing lentiviruses were used to evaluate the role of *Fzd6* in the osteogenic differentiation of OP-ASCs. Real-time PCR (qPCR) and western blotting (WB) was performed to detect the expression of *Fzd6* and bone-related molecules, including runt-related transcription factor 2 (*Runx2*) and osteopontin (*Opn*). Alizarin red staining and Alkaline phosphatase (ALP) staining was performed following osteogenic induction. Microscopic CT (Micro-CT), hematoxylin and eosin staining (H&E) staining, and Masson staining were used to assess the role of *Fzd6* in osteogenic differentiation of osteoporosis (OP) mice *in vivo*.

Results: Expression of *Fzd6* was decreased significantly in OP-ASCs. *Fzd6* silencing down-regulated the osteogenic ability of OP-ASCs *in vitro*. Overexpression of *Fzd6* rescued the impaired osteogenic capacity in OP-ASCs *in vitro*. We obtained similar results *in vivo.*

Conclusions: *Fzd6* plays an important role in regulating the osteogenic ability of OP-ASCs both *in vivo* and *in vitro*. Overexpression of *Fzd6* associated with the Wnt signaling pathway promotes the osteogenic ability of OP-ASCs, which provides new insights for the prevention and treatment of OP.

1 Introduction

OP is a disease characterized by abnormal bone metabolism, trabecular bone structure disorders, and bone loss, which can lead to increased bone fragility [1, 2]. As the homeostasis between osteoblasts and osteoclasts is destroyed, bone resorption by osteoclasts becomes faster than bone formation by osteoblasts, which leads to a decrease in bone mass and an increase in bone fragility, thus increasing the risk of fracture [3, 4]. OP is more prevalent in women than men, especially in postmenopausal women, whose bone metabolism is accelerated because of estrogen deficiency [5]. OP seriously affects the quality of life of postmenopausal women, and nearly 50% of women may experience osteoporotic fractures after menopause [6]. At present, the number of people suffering from OP is increasing, and OP has become a major disease worldwide that seriously impacts people's health [7, 8]. Many researchers are currently focusing on the issues of reducing bone damage and repairing bone defects in OP.

In recent years, bone tissue engineering has become a topic of interest for repairing bone defects and has explored the combination of seed cells, biological scaffold materials, and bioactive molecules to promote osteogenesis [9, 10]. Bone marrow mesenchymal stem cells (BMSCs) are attractive for the treatment of osteoporotic bone defects, but in elderly patients with OP, BMSCs tend to differentiate into adipocytes rather than osteoblasts [11]. Furthermore, bone marrow aspiration to obtain BMSCs is an extremely

painful process, and the number of cells obtained is usually low [12, 13]. ASCs can also differentiate into osteoblasts and chondrocytes [14–17]. Because of their ability to multi-directionally differentiate, their extensive proliferative capacity, and low immunogenicity, ASCs have become an attractive source of seed cells for regenerative medicine and tissue engineering [18–22]. Therefore, researchers hope to transplant autologous ASCs from osteoporotic patients for the treatment of bone defects. However, the osteogenic differentiation potential of OP-ASCs is significantly impaired compared with ASCs [23]. Moreover, the mechanisms associated with the reduced osteogenic capacity of OP-ASCs are not clear.

The Wnt signaling pathway plays an important role in the regulation of bone differentiation and bone formation by ASCs [15, 24]. Wnt proteins can activate downstream pathways by binding to the corresponding Frizzled (FZD) receptors, including Wnt/β-catenin, Wnt/planar cell polarity, and Wnt/Ca^{2+} [25]. Due to its unique seven transmembrane structure, FZD is the link to the Wnt signaling pathway from the extracellular to the intracellular, and it is an important part of Wnt signaling pathway [26, 27]. Among the members of the FZD family, *Fzd6* is broadly expressed in various tissues [28]. Cvjetkovic N et al [29] found that *Fzd6* down-regulates the activity of the TCF/LEF complex through the Wnt/Ca^{2+} signaling pathway to inhibit the canonical Wnt signaling pathway. Abuna RPF et al [30] found that *Fzd6* enhanced the high osteogenicity of nanotopography by activating the canonical Wnt/β-catenin signaling pathway. Olivares-Navarrete et al [31] demonstrated that the up-regulation of *Fzd6* associated with the non-canonical Wnt signaling pathway in osteoblasts to improve osteogenic properties *in vitro*. However, the regulatory mechanism of *Fzd6* in the differentiation of OP-ASCs into osteoblasts has not been reported.

In this study, gene chip data suggested that the expression of *Fzd6* was decreased in OP-ASCs after the induction of osteogenesis. Based on the literature and our previous work, we hypothesized that *Fzd6* may have a positive impact on the physiological functions of OP-ASCs through the Wnt signaling pathway. This study aimed to explore the effects of *Fzd6* on the osteogenic ability of OP-ASCs through the overexpression or silencing of *Fzd6*. Moreover, *Fzd6* can be used as a specific therapeutic target to treat osteoporotic bone defects.

2 Materials And Methods

2.1 Experimental Materials

2.1.1 Experimental Animals

Thirty 8-week-old C57BL/6 female mice were purchased from ChongQing TengXin Biological Technology Co., Ltd. (ChongQing, China). Each mouse had a body weight of about 18 g.

2.2 Experimental Method

2.2.1 Establishment of Osteoporotic Mouse Model

Ovariectomy (OVX) was performed when the weight of each mouse reached 20 g. The mice were weighed and anaesthetized by intraperitoneal injection of 1% sodium pentobarbital (30 mg/kg). After the removal of the bilateral ovaries, the abdominal muscle tissue and skin were sutured.

2.2.2 Isolation and Culture of OP-ASCs

OP-ASCs were obtained from the subcutaneous fat at the inguinal sites of the op mice. Adipose tissue was washed with 10% penicillin-streptomycin PBS, 5% penicillin-streptomycin PBS, and penicillin-streptomycin-free PBS in turn. Then, adipose tissue were seeded in 25 cm^2 culture flasks with modified eagle's medium and were cultured in an atmosphere of 5% CO_2 at 37 °C for 5 days. Adherent adipose tissue were cultured in a monolayer and non-adherent adipose tissue were removed. The medium was substituted for fresh medium every 3 days and cells were subcultured upon reaching 80% confluence. Cells were passaged three times in the subsequent experiments.

2.2.3 PCR Gene Chip Screening of Wnt Signaling Pathway Gene Changes in ASCs and OP-ASCs

OP-ASCs and ASCs were cultured. Total RNA was extracted from the LiCl group (50 mg/mL LiCl), DKK-1 group (0.1 μg/mL DKK-1), and control group at day 1 and day 3. Genes related to the Wnt signaling pathway were then screened by Wnt signaling pathway gene chip combined with qPCR.

2.2.4 Expression of *Fzd6* mRNA and Protein in OP-ASCs

The mRNA expression of *Fzd6* was assessed by qPCR and protein expression of FZD6 was detected by WB.

2.2.5 Construction of Lentivirus-mediated Overexpression and Silencing of *Fzd6*

The construction, sequencing, purification and titer determination of lentivirus vectors were completed by Heyuan Biotechnology Co., Ltd. All lentivirus vectors contained green fluorescent protein (GFP) and puromycin resistance genes. Lentivirus-mediated overexpression of *Fzd6* carried *3-Flag*, while the other groups did not carry *3-Flag*. *3-Flag* can be used to verify the successful transfection of lentivirus. The efficiency of successful transfection was verified by fluorescence microscopy.

2.2.6 Determination of Lentivirus Multiplicity of Infection (MOI)

The lentiviruses evaluated included *Fzd6*(+), *Fzd6*(-), shRNA-1, shRNA-2, shRNA-3, and shRNA(-). The MOI value was set using the following gradient: 0, 20, 40, 60, 80, 100. The volume of virus solution needed in each group was calculated according to the following formula: virus volume = cell number × MOI/virus titer. After transfection for 72 h, the morphology and fluorescence expression of the cells was observed and recorded by fluorescence microscopy to determine the optimal MOI value for each lentivirus.

2.2.7 Acquisition of OP-ASCs Stably Transfected with Lentivirus-mediated Overexpression or Silencing of *Fzd6*

Lentivirus transfection was performed when the optimal MOI value was 80. After 72 h of transfection, stably transfected cells were selected with 0.6 μg/mL of puromycin.

2.2.8 Cell Viability Assays

Second-passage OP-ASCs (5×10^5 cells per 1 mL) and BCP were co-cultured in 96-well plates. Cell proliferation was measured by cell counting kit-8 (CCK-8, Solarbio, China) at 1 d, 3 d, 5 d, and 7 d. The absorbance of each sample was measured at 450 nm by a microplate reader (Spectra Thermo, Switzerland).

2.2.9 Proliferation and Adhesion of OP-ASCs on BCP was Detected by Scanning Electron Microscope (SEM)

BCP was placed in 24-well plates and 1 mL second-passage OP-ASCs cell suspension (5×10^5 cells per mL) was added to the surface of the BCP in each well. 24-well plates were cultured in 5% CO_2 at 37°C. Samples were fixed with paraformaldehyde on the 3rd and 7th day of culture. Alcohol gradient dehydration and critical point drying were then performed and cells were sprayed with gold for SEM observation.

2.2.10 Osteogenic Induction

OP-ASCs were seeded onto 6-well plates at a density of 5×10^4 cells/mL. The medium was changed to osteogenic induction medium (Cyagen, Guangzhou, China) when OP-ASCs reached a fusion of 80%.

2.2.11 Alkaline Phosphatase Staining (ALP) and Alizarin Red Staining

After osteogenic induction for 7 days, OP-ASCs transfected with *Fzd6* lentivirus were rinsed with PBS and fixed with 4% paraformaldehyde at 4°C for 30 minutes. ALP activity was detected using an Alkaline Phosphatase Assay Kit (Beyotime, Shanghai, China).

After 14 days of osteogenic induction, OP-ASCs were washed three times with PBS and fixed with 4% paraformaldehyde at room temperature for 30 minutes. Cells were then rinsed three times with PBS and incubated in 0.1% Alizarin red staining for 15 minutes at 37°C.

2.2.12 Extraction of RNA and qPCR

Total cellular RNA was isolated using the Total RNA Extraction Kit (Tiangen, Shanghai, China) and subsequently reverse transcribed into cDNA using the RevertAid First Strand cDNA Synthesis Kit (Thermo, Waltham, USA). All primers in this study were synthesized by Shenggong Bioengineering Co., Ltd (Shanghai China). The specific primer sequences were as follows: *Gapdh*, (forward) 5'-GGGTGAAGGTCGGTGTGAACG-3' and (reverse) 5'-CTCGCTCCTGGAAGATGGTG-3'; *Fzd6*, (forward) 5'-

AGACAACATTAGCGGCGTTT-3' and (reverse) 5'-AGAGGAGAGACAGCCCAACA-3'; *Runx2*, (forward) 5'-CCGAACTGGTCCGCACCGAC-3' and (reverse) 5'-CTTGAAGGCCACGGGCAGGG-3'; *Opn*, (forward) 5'-GGATTCTGTGGACTCGGATG-3' and (reverse) 5'-CGACTGTAGGGACGATTGGA-3'. The qPCR reaction was in accordance with the instructions of QuantiNova SYBR Green PCR Kit. The reaction system was added to qPCR 96-well plates. The reaction liquid was collected at the bottom of the plate by horizontal centrifugation and the plate was then placed in a real-time PCR instrument. After the reaction was completed, the amplification curve and dissolution curve of each gene was analyzed by 7900 System SDS software and the relative expression of the target genes was calculated and statistically analyzed.

2.2.13 Western Blotting Assay

Proteins were separated by 10% sodium dodecylsulfate polyacrylamide gel electrophoresis (SDS-PAGE) and then transferred to polyvinylidene difluoride (PVDF) membranes. After blocking with 5% skim milk for 1 h at 37°C, the membranes were incubated with primary rabbit monoclonal antibodies specific to the following targets: GAPDH (ab181602), 3-FLAG (ab125243), FZD6 (ab98933), OPN (ab8448), and RUNX2 (ab92336) (Abcam, Cambridge, UK). Then, each membrane was incubated with a secondary labeled anti-rabbit antibody (Beyotime, Shanghai, China). Membranes were developed using an enhanced chemiluminescence detection system (Bio-Rad, Hercules, USA).

2.2.14 BCP Combined with OP-ASCs was Transplanted into a Mouse Model of Critical-sized Calvarial Defects

OP-ASCs transfected with *Fzd6* overexpression lentivirus, silencing lentivirus, or untransfected lentivirus were prepared and cultured in osteogenic induction medium. 1 mL cell suspension (5×10^5 cells per 1 mL) was added to the surface of the BCP in 24-well plates. 24-well plates were cultured in a CO_2 incubator for 48 h. The osteoporosis mice were treated with prone fixation, skin preparation, and disinfection at the top of the skull. The skin was cut at the midline of the skull, the skull was exposed, and the periosteum was bluntly separated. Then, full-thickness defects of 4 mm were created symmetrically. The BCP combined with OP-ASCs was transplanted into the skull defect area and the operation area was then sutured. After 4 and 8 weeks, mice were euthanized and the skull specimens were obtained.

2.2.15 Micro-CT, H&E staining, and Masson staining

Micro-CT scans were performed on mice with skull defects at 4 and 8 weeks. Then, tissues samples of mice skull defect were stained with H&E and Masson staining.

2.3 Statistical Analysis

All experiments were repeated a minimum of three times independently, and representative data are provided as mean ± the standard deviation (SD). Differences between two groups were analyzed by student's independent t-test, while differences between multiple groups were analyzed by one-way analysis of variance (ANOVA). Statistical analysis was completed using SPSS 20.0 software. Differences were accepted as statistically significant if $P < 0.05$.

3 Results

3.1 Primary Culture and Subculture of OP-ASCs

The OP-ASCs of generation P0 were passaged to generations P1 and P2 (Fig. 1A). The cell morphologies remained stable and uniform.

3.2 Osteogenic Differentiation Potential of OP-ASCs

Second-passage OP-ASCs were cultured in 6-well plates. After 14 days of induced osteogenesis, many mineralized nodules were observed (Figure. 1B). The cells were tightly arranged and the cell morphology was polygonal or oval.

3.3 The Results of Gene Chip

Gene chip data showed that many genes related to the Wnt signaling pathway changed after osteoinduction in ASCs and OP-ASCs. Interestingly, *Fzd6* expression was significantly decreased (Fig. 2).

3.4 Gene and Protein Expression of *Fzd6* in OP-ASCs

Fzd6 gene expression was decreased in OP-ASCs (Fig. 3A). The protein expression of FZD6 was also significantly decreased in OP-ASCs (Fig. 3B).

3.5 Optimal MOI Value of *Fzd6* Lentivirus

Fluorescence expression was observed by inverted fluorescent microscope at 72 h after transfection. At a MOI value of 80, fluorescence expression was strongest in the [*Fzd6*(+)], [shRNA(+)-1], [shRNA(+)-2] and [shRNA(+)-3] groups. For [shRNA(+)-1], the morphology of the cells was poor (Fig. 4). Therefore, [shRNA(+)-2] and [shRNA(+)-3] lentiviruses were used for subsequent experiments.

3.4 qPCR Verified the Successful Transfection of *Fzd6* Overexpression or Silencing Lentivirus

The gene expression of *Fzd6* in cells transfected with [*Fzd6*(+)] lentivirus was significantly higher than in control groups. However, in [shRNA(+)-2] and [shRNA(+)-3] transfected cells, *Fzd6* expression was significantly decreased. The expression of *Fzd6* was no difference between the [*Fzd6*(-)] and [shRNA(-)] groups compared with the control group (Fig. 5A).

3.5 WB Verified the Successful Transfection of *Fzd6* Overexpression or Silencing Lentivirus

While the overexpression group contained 3-FLAG tag protein, no 3-FLAG tag protein was found in the other groups, which could support that *Fzd6* lentivirus was successfully transferred into OP-ASCs and

integrated *3-Flag* into the OP-ASC genome. The protein expression of FZD6 in the overexpression group was significantly higher than in the control group, while in the [shRNA(+)-2] and [shRNA(+)-3] groups, the expression of FZD6 was significantly lower. The expression of FZD6 was no statistically significant difference in [*Fzd6*(-)] and [shRNA(-)] compared with the control group (Fig. 5B).

3.6 The Osteogenic Ability of OP-ASCs was Detected by qPCR and WB

OP-ASCs stably transfected with *Fzd6* lentivirus were induced into osteogenesis. The mRNA expression of *Fzd6*, *Runx2*, and *Opn* in the [*Fzd6*(+)] group increased significantly after 3 days of osteogenic induction, while the expression of *Fzd6*, *Runx2*, and *Opn* decreased significantly in [shRNA(+)] (Fig. 6A). The protein expression of FZD6, RUNX2, and OPN was significantly higher in [*Fzd6*(+)] (Fig. 6B). After 5 days of osteogenic induction, the mRNA expression of *Fzd6*, *Runx2*, and *Opn* was also increased in [*Fzd6*(+)] (Fig. 6C). The protein expression of FZD6, RUNX2, and OPN was significantly increased in [*Fzd6*(+)]. However, these proteins were significantly decreased in [shRNA(+)] (Fig. 6D).

3.7 The Osteogenic Ability of OP-ASCs was Detected by ALP Staining and Alizarin Red Staining

ALP staining was performed on day 7. The results showed the most alkaline phosphatase in [*Fzd*6(+)] and the least alkaline phosphatase in [shRNA(-)] (Figure. 7A). Alizarin red staining was performed on day 14 (Fig. 7B) and showed that the formation of mineralization nodules increased in [*Fzd6*(+)]. However, the formation of mineralization nodules decreased in [shRNA(+)].

3.8 CCK-8 Assay for the Detection of the Proliferation of OP-ASCs and Cytotoxicity of BCP

OP-ASCs and BCP were co-cultured for 1 d, 3 d, 5 d, and 7 d and the proliferation of OP-ASCs and cytotoxicity of BCP were detected by CCK-8 assay. The results (Fig. 8A) showed that the number of cells gradually increased as the length of co-culture time increased. These results indicated that OP-ASCs could grow and proliferate in an environment with BCP and that BCP had no cytotoxic effect on OP-ASCs.

3.9 Proliferation and Adhesion of OP-ASCs on the BCP Surface was Detected by SEM

The proliferation and adhesion of OP-ASCs on the surface of BCP was detected by SEM. The results showed that OP-ASCs grew adherently on the surface and pores of BCP. On day 3 (Fig. 8B) and day 7 (Fig. 8C) of co-culture, the number of cells increased and the extracellular matrix was gradually connected into pieces.

3.10 Micro-CT was Used to Detect the Osteogenic Capacity of OP-ASCs *in Vivo*

Four weeks after the transplantation of OP-ASCs and BCP in the skull defect area, three-dimensional reconstruction of Micro-CT scan showed that the green part of BCP was the new bone matrix. The amount of green bone matrix observed was significantly higher in [*Fzd6*(+)] and was significantly lower in [shRNA(+)] (Fig. 9A). Through sagittal, coronal, and BV/TV analysis (Fig. 9C), we found that the osteogenic ability of [*Fzd6*(+)] was significantly increased, while the osteogenic ability of [shRNA(+)] was significantly decreased.

Eight weeks after transplantation of OP-ASCs, three-dimensional reconstruction showed that the amount of green bone matrix observed was significantly higher than at four weeks, and the amount of green bone matrix observed was significantly higher in [*Fzd6*(+)] (Fig. 9B). The results showed that the osteogenic ability of OP-ASCs was significantly increased in [*Fzd6*(+)] (Fig. 9C).

3.11 H&E and Masson Staining were Used to Detect Osteogenic Ability of OP-ASCs in Vivo

Four weeks after transplantation of OP-ASCs and BCP in the skull defect area, the osteogenic ability of OP-ASCs was detected by H&E and Masson staining. H&E staining showed that the new bone matrix was red, and the staining degree of [*Fzd6*(+)] was deeper than that of [shRNA(+)]. Additionally, Masson staining showed that the new bone matrix was blue, and the staining degree was deeper in [*Fzd6*(+)] (Fig. 10A). Eight weeks after the implantation of OP-ASCs, similar results were obtained (Fig. 10B).

4 Discussion

OP is a major disease worldwide, and the prevention and treatment of osteoporotic bone defects continues to be an area of focus in bone tissue engineering research [32]. At present, composite scaffolds combined with autologous stem cells could effectively repair osteoporotic bone defects [33, 34]. ASCs are ideal substitutes for BMSCs because of their larger storage capacity, easier acquisition, richer source, and lower immunogenicity [20, 35–37]. ASCs can grow on plastic petri dishes and proliferate actively, and can differentiate into a variety of cells, including osteoblasts, adipocytes, cartilage cells, muscle cells, and ligament cells [38–40]. Thus, ASCs may be one of the most promising cell types for bone regeneration in bone tissue engineering [41]. Cho et al found that the therapeutic effect of ASCs was similar to that of estrogen therapy and could prevent bone loss in OVX mice [42]. Mirsaidi et al treated elderly osteoporosis mice with autologous ASCs and found that osteogenesis related molecules were significantly increased and the quality of bone trabecula was significantly improved [43]. These studies suggest that autologous ASCs transplantation is an effective cell therapy for osteoporosis fractures and bone defects. Therefore, transplantation of OP-ASCs into an area of bone defect may be a potential treatment for osteoporosis patients. However, a previous study found that the osteogenic differentiation potential of OP-ASCs is significantly impaired compared with ASCs [23]. Thus, it is worthwhile to improve the osteogenic ability of OP-ASCs and enhance the bone formation in the bone defect area after the transplantation of OP-ASCs.

Nevertheless, there are currently few studies exploring the mechanisms underlying the decreased osteogenic ability of OP-ASCs and strategies to improve the osteogenic ability of these cells.

In this study, we established a mouse model of OP and obtained OP-ASCs. Consistent with previous studies, Alizarin red staining showed that many mineralized nodules were present in these cells [35]. This result demonstrates that OP-ASCs can proliferate, self-renew, and differentiate to bone, and therefore can be used as seed cells for the treatment of osteoporotic bone defects. Next, we screened out differentially expressed genes related to the Wnt signaling pathway in OP-ASCs and ASCs through PCR gene chip. After analyzing the chip data results, we found that *Fzd6* decreased significantly in OP-ASCs. Additionally, we found that the gene and protein level of *Fzd6* was also reduced in OP-ASCs. Therefore, we aimed to investigate the osteogenic effect of *Fzd6* on OP-ASCs and explore changes in the osteogenic capacity of OP-ASCs through the up-regulation and down-regulation of *Fzd6*.

The Wnt signaling pathway plays an important regulatory role in the process of osteogenic differentiation in ASCs and BMSCs [15, 44]. Additionally, the WNT/FZD signaling pathway plays a vital role in the repair, regeneration, and plasticity of adult bone tissue [45–47]. Boland GM et al [48] found that *Fzd6* was up-regulated in the process of osteogenic differentiation in BMSCs *in vitro*. This result suggested that an increase in *Fzd6* expression may activate the Wnt signaling pathway and promote the expression of downstream target genes and thereby promote osteogenesis. Vlacic-Zischke J et al [49] found that on the surface of hydrophilic titanium implants, the osteogenic ability of osteoblasts was significantly enhanced and the expression of *Fzd6* in the Wnt signaling pathway was significantly increased. This result indicated that the enhanced osteogenic ability of osteoblasts may be the result of up-regulation of *Fzd6* in the Wnt signaling pathway. However, there are currently few studies that involve the direct regulation of changes in *Fzd6* expression and subsequent observation of the effect of these changes on osteogenesis. In the present study, we investigated the effect of the overexpression or silencing of *Fzd6* on the osteogenic potential of OP-ASCs. We found that silencing *Fzd6* in OP-ASCs decreased the expression of osteogenic-related regulation factor *Runx2* and *Opn* during the process of bone formation. After overexpression of *Fzd6*, the expression of *Runx2* and *Opn* increased over time. Furthermore, ALP staining and Alizarin red staining showed that silencing *Fzd6* reduced the early and late osteogenic differentiation capacities of OP-ASCs. Conversely, overexpression of *Fzd6* partially rescued the early and late osteogenic differentiation capacities of OP-ASCs. Correlation analysis determined that *Fzd6* could up-regulate the osteogenic differentiation capacity of OP-ASCs *in vitro*. Therefore, we assert that *Fzd6* regulates the osteogenic capacity of OP-ASCs.

It is worth noting that the osteogenic effects of *Fzd6* in the regulation of OP-ASCs need to be further confirmed *in vivo*. Ye X et al [50] wrapped autologous ASCs with calcium alginate gel and implanted them into the distal femur of OVX rabbits and found that the femoral bone mineral density of OVX rabbits in the composite ASCs group increased significantly and promoted the formation of new bone. BCP is a new type of biological scaffold material that provides sufficient space for cell attachment, growth, and proliferation [51, 52]. Rath SN et al found that BMSCs can proliferate on BCP and promote bone formation following osteogenic induction [53]. In the present study, BCP combined with OP-ASCs was

transplanted into a mouse critical-sized calvarial defect model for *in vivo* osteogenesis studies. Micro-CT reconstructed images showed that the formation of new bone increased with time in each group of composite BCP, and the [*Fzd6*(+)] group had the most new bone during the observed time period. These results indicate that overexpression of *Fzd6* can partially rescue the decline in osteogenic ability of OP-ASCs. Furthermore, histological observations of the corresponding tissue samples were also consistent with the results of Micro-CT ,that is, the amount of new bone formation of [*Fzd6*(+)] is more obvious than the amount of new bone formation of [shRNA(+)]. These findings suggest that *Fzd6* can rescue the reduced osteogenic ability of OP-ASCs, and is a potential therapeutic target for the prevention and treatment of osteoporosis.

5 Conclusion

This study shows that the overexpression of *Fzd6* can promote the osteogenic potential of OP-ASCs and rescue the decline in osteogenesis of OP-ASCs. Silencing *Fzd6* effectively reduces the osteogenesis of OP-ASCs. Furthermore, given the role of *Fzd6* as a key factor related to osteogenic regulation by the Wnt signaling pathway, *Fzd6* could serve as an important target for the treatment of bone defects in OP.

Declarations

FundingThis work was funded by National Natural Science Foundation of China (81870746, 81700976), Joint project of Luzhou Municipal People's Government and Southwest Medical University (2020LZXNYDZ09), and Natural Science Foundation of Shanghai (17ZR1432700).

Authors ContributionsTL.W. and ZH.Y. established OP animal model, performed *in vitro* and *in vivo* experiments, executed the analysis of the data, and drafted the manuscript. G.T. reviewed and revised the manuscript. FZ.L., H.T. and YJ.G. collected the data. XJ.Y. designed experimental project, analyzed data and revised manuscript. JG.X. initiated study, designed experimental project, analyzed data, revised manuscript and provided funding. All authors have seen and approved the manuscript.

Data Availability The data which support research results are available from the corresponding author upon reasonable request.

Ethical Approval All animal experimental procedures were reviewed and approved by Southwest Medical University Ethical Committee (20180391222). Animal experiments were conducted in accordance with the guidelines for the Care and Use of Laboratory Animals (Ministry of Science and Technology of China, 2006).

Consent to Participate Not Applicable.

Consent to Publish Not Applicable.

Competing Interests The authors declare no conflict of interests.

References

1. Zhang L, Yin X, Wang J, et al. (2018). Associations between VDR Gene Polymorphisms and Osteoporosis Risk and Bone Mineral Density in Postmenopausal Women: A systematic review and Meta-Analysis[J]. *Sci Rep, 8*(1):981.
2. Matsushita M, Mishima K, Yamashita S, et al. (2020). Impact of fracture characteristics and disease-specific complications on health-related quality of life in osteogenesis imperfecta[J]. *J Bone Miner Metab. 38*(1):109-116.
3. Hu L, Yin C, Zhao F, et al. (2018). Mesenchymal Stem Cells: Cell Fate Decision to Osteoblast or Adipocyte and Application in Osteoporosis Treatment[J]. *Int J Mol Sci, 19*(2). pii: E360.
4. Chen XF, Li XL,Yang M,et al. (2018).Osteoprotective effects of salidroside in ovariectomized mice and diabetic mice[J]. *Eur J Pharmacol, 819*:281-288.
5. Chen XF, Li XL,Yang M,et al. (2018).Osteoprotective effects of salidroside in ovariectomized mice and diabetic mice[J]. *Eur J Pharmacol, 819*:281-288.
6. Mollard E, Bilek L, Waltman N. (2017). Emerging evidence on the link between depressive symptoms and bone loss in postmenopausal women[J]. *Int J Womens Health, 28*(10):1-9.
7. Woisetschläger M, Spångeus A. (2018). Model for improved correlation of BMD values between abdominal routine Dual energy CT data and DXA scans[J]. *Eur J Radiol, 99*:76-81.
8. Weisgerber DW, Milner DJ, Lopez-Lake H, et al. (2018). A Mineralized Collagen-Polycaprolactone Composite Promotes Healing of a Porcine Mandibular Defect[J]. *Tissue Eng Part A, 24*(11-12):943-954.
9. Fu N, Meng Z, Jiao T, et al. (2019). P34HB electrospun fibres promote bone regeneration *in vivo*. *Cell Prolif, 52*(3):e12601.
10. Song F, Sun H, Huang L, et al. (2018). The Role of Pannexin3-Modified Human Dental Pulp-Derived Mesenchymal Stromal Cells in Repairing Rat Cranial Critical-Sized Bone Defects[J]. *Cell Physiol Biochem, 44*(6):2174-2188.
11. Dufrane D. (2017). Impact of Age on Human Adipose Stem Cells for Bone Tissue Engineering [J]. *Cell Transplant, 26*(9):1496-1504.
12. Guilak F, Lott KE, Awad HA, et al. (2006). Clonal analysis of the differentiation potential of human adipose-derived adult stem cells[J]. *J Cell Physiol, 206*(1):229-37.
13. Rodriguez AM, Elabd C, Amri EZ, et al. (2005). The human adipose tissue is a source of multipotent stem cells[J]. *Biochimie, 87*(1):125-8.
14. Dawn B, Bolli R. (2005). Adult bone marrow-derived cells: regenerative potential, plasticity, and tissue commitment[J]. *Basic Res Cardiol, 100*(6):494-503.
15. Li KC, Chang YH, Hsu MN, et al. (2018). Baculovirus-Mediated miR-214 Knockdown Shifts Osteoporotic ASCs Differentiation and Improves Osteoporotic Bone Defects Repair[J]. *Sci Rep7*(1):16225.

16. Ciuffi S, Zonefrati R, Brandi ML. (2017). Adipose stem cells for bone tissue repair [J]. *Clin Cases Miner Bone Metab, 14*(2):217-226.
17. Zhang Y, Lei Z, Qi Y, et al. (2017). Adipose-derived stem cell sheet encapsulated construct of micro-porous decellularized cartilage debris and hydrogel for cartilage defect repair[J]. *Med Hypotheses, 109*:111-113.
18. Tajima S, Tobita M, Mizuno H. (2017). Current status of bone regeneration using adipose-derived stem cells[J]. *Histol Histopathol, 2*:11942.
19. Zhang WB, Zhong WJ, Wang L. (2014). A signal-amplification circuit between miR-218 and Wnt/β-catenin signal promotes human adipose tissue-derived stem cells osteogenic differentiation[J]. *Bone, 58*:59-66.
20. Cai X, Xie J, Yao Y, et al. (2017). Angiogenesis in a 3D model containing adipose tissue stem cells and endothelial cells is mediated by canonical Wnt signaling[J]. *Bone Res, 5*:17048.
21. Shafaei H, Kalarestaghi H, et al. (2020) Adipose-derived stem cells: An appropriate selection for osteogenic differentiation. *J Cell Physiol. 235*(11):8371-8386.
22. Jeong W, Kim YS, et al. (2020) The effect of combination therapy on critical-size bone defects using non-activated platelet-rich plasma and adipose-derived stem cells. *Childs Nerv Syst. 36*(1):145-151.
23. Wang L, Huang C, Li Q, et al. (2017). Osteogenic differentiation potential of adipose-derived stem cells from ovariectomized mice. *Cell Prolif. 50*(2):e12328.
24. Yang S, Guo S, Tong S, et al. (2020). Exosomal miR-130a-3p regulates osteogenic differentiation of Human Adipose-Derived stem cells through mediating SIRT7/Wnt/β-catenin axis. *Cell Prolif. 53*(10):e12890.
25. Dijksterhuis JP, Petersen J, Schulte G. (2014). WNT/Frizzled signalling: receptor-ligand selectivity with focus on FZD-G protein signalling and its physiological relevance: IUPHAR Review 3[J]. *Br J Pharmacol, 171*(5):1195-209.
26. DeBruine ZJ, Xu HE, Melcher K. (2017). Assembly and architecture of the Wnt/β-catenin signalosome at the membrane[J]. *Br J Pharmacol, 174*(24):4564-4574.
27. Kozielewicz P, Hoffmann C, Schulte G, et al. (2020). Structural insight into small molecule action on Frizzleds[J]. *Nat Commun. 11*(1):414.
28. Kim BK, Yoo HI, Kim I, et al. (2015). FZD6 expression is negatively regulated by miR-199a-5p in human colorectal cancer. *BMB Rep, 48*(6):360-6.
29. Cvjetkovic N, Maili L, Weymouth KS, et al. (2015). Regulatory variant in FZD6 gene contributes to nonsyndromic cleft lip and palate in an African-American family[J]. *Mol Genet Genomic Med, 3*(5):440-451.
30. Abuna RPF, Oliveira FS, Adolpho LF, et al. (2020). Frizzled 6 disruption suppresses osteoblast differentiation induced by nanotopography through the canonical Wnt signaling pathway. *J Cell Physiol. 235*(11):8293-8303.

31. Chakravorty N, Ivanovski S, Prasadam I, et al. (2018) The microRNA expression signature on modified titanium implant surfaces influences genetic mechanisms leading to osteogenic differentiation. *Acta Biomater. 8*(9):3516-23.
32. Dubey NK, Mishra VK, Deng WP, et al. (2018). Revisiting the Advances in Isolation, Characterization and Secretome of Adipose-Derived Stromal/Stem Cells[J]. *Int J Mol Sci. 19*(8):2200.
33. Ma W, Zhan Y, Zhang Y, et al. (2020). Enhanced Neural Regeneration with a Concomitant Treatment of Framework Nucleic Acid and Stem Cells in Spinal Cord Injury. *ACS Appl Mater Interfaces. 12*(2):2095-106.
34. Cao L, Liu G, Gan Y, et al. (2012) The use of autologous enriched bone marrow MSCs to enhance osteoporotic bone defect repair in long-term estrogen deficient goats. *Biomaterials. 33*:5076–5084.
35. Dominici M, Le Blanc K, Mueller I, et al. (2006). Minimal criteria for defining multipotent mesenchymal stromal cells. The International Society for Cellular Therapy position statement[J]. *Cytotherapy, 8*(4):315-7.
36. Zuk P.A, Zhu M, Mizuno H, et al. (2001). Multilineage cells from human adipose tissue: implications for cell-based therapies[J]. *Tissue Eng, 7*(2):211-228.
37. Gimble JM, Katz AJ, Bunnell BA. (2007). Adipose-derived stem cells for regenerative medicine[J]. *Circ Res, 100*(9):1249-60.
38. Gentile P, Sterodimas A. (2020). Adipose-derived stromal stem cells (ASCs) as a new regenerative immediate therapy combating coronavirus (COVID-19)-induced pneumonia[J]. *Expert Opin Biol Ther. 20*(7):711-716.
39. Ma Q, Liao J, Cai X, et al. (2018). Different Sources of Stem Cells and their Application in Cartilage Tissue Engineering. *Curr Stem Cell Res Ther. 13*(7):568-75.
40. Gu X, Li C, Yin F, et al. (2017). Adipose-derived stem cells in articular cartilage regeneration: current concepts and optimization strategies[J]. *Histol Histopathol, 15*:11955.
41. Arnhold S, Klymiuk MC, Geburek F, et al. (2017). Investigation of stemness and multipotency of equine adipose-derived mesenchymal stem cells (ASCs) from different fat sources in comparison with lipoma[J]. *Stem Cell Res Ther. 22*;10(1):309.
42. Cho SW, Sun HJ, Yang JY, et al. (2012). Human adipose tissue-derived stromal cell therapy prevents bone loss in ovariectomized nude mouse[J]. *Tissue Eng Part A, 18*(9-10):1067-78.
43. Mirsaidi A, Genelin K, Vetsch JR, et al. (2014). Therapeutic potential of adipose-derived stromal cells in age-related osteoporosis[J]. *Biomaterials, 35*(26):7326-35.
44. Li Y, Wang L, Zhang M, et al. (2020). Advanced glycation end products inhibit the osteogenic differentiation potential of adipose-derived stem cells by modulating Wnt/β-catenin signalling pathway via DNA methylation. *Cell Prolif. 53*(6):e12834.
45. Logan CY, Nusse R. (2004). The Wnt signaling pathway in development and disease[J]. *Annu Rev Cell Dev Biol,20*:781-810.

46. Van Amerongen R, Nusse R. (2009). Towards an integrated view of Wnt signaling in development[J]. *Development, 136*(19):3205-14.
47. Chien AJ, Conrad WH, Moon RT. (2009). A Wnt survival guide: from flies to human disease[J]. *J Invest Dermatol, 129*(7):1614-27.
48. Boland GM, Perkins G, Hall DJ, et al. (2004). Wnt3a promotes proliferation and suppresses osteogenic differentiation of adult human mesenchymal stem cells[J]. *J Cell Biochem, 93*(6):1210-30.
49. Vlacic-Zischke J, Hamlet SM, Friis T, et al. (2011). The influence of surface microroughness and hydrophilicity of titanium on the up-regulation of TGFβ/BMP signalling in osteoblasts[J]. *Biomaterials, 32*(3):665-71.
50. Ye X, Zhang P, Xue S, et al. (2014). Adipose-derived stem cells alleviate osteoporosis by enhancing osteogenesis and inhibiting adipogenesis in a rabbit model[J]. *Cytotherapy, 16*(12):1643-55.
51. Wu J, Chen T, Wang Z, Chen X, et al. (2020). Joint construction of micro-vibration stimulation and BCP scaffolds for enhanced bioactivity and self-adaptability tissue engineered bone grafts. *J Mater Chem B. 21*;8(19):4278-4288.
52. X.D. Zhu, H.J. Zhang, H.S. Fan, et al. (2010). Effect of phase composition and microstructure of calcium phosphate ceramic particles on protein adsorption. *Acta Biomater. 6*:1536–1541.
53. Rath SN, Strobel LA, Arkudas A, et al. (2010). Osteoinduction and survival of osteoblasts and bone-marrow stromal cells in 3D biphasic calcium phosphate scaffolds under static and dynamic culture conditions. *J Cell Mol Med. 16*(10):2350-61.

Figures

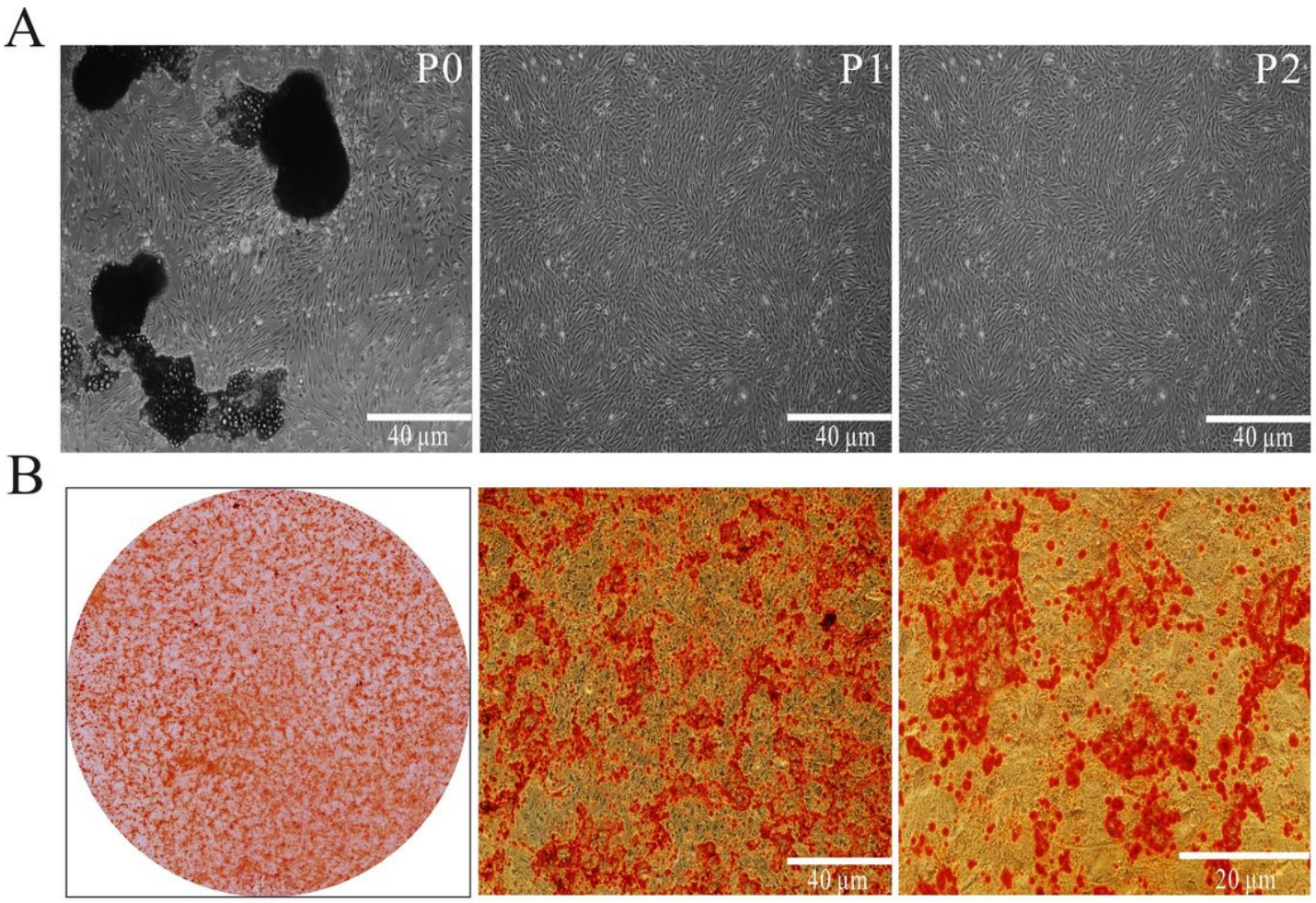

Figure 1

Isolation and culture OP-ASCs. (A) The primary culture and subculture of OP-ASCs. (B) Alizarin red staining of OP-ASCs on the 14th day after osteogenic induction.

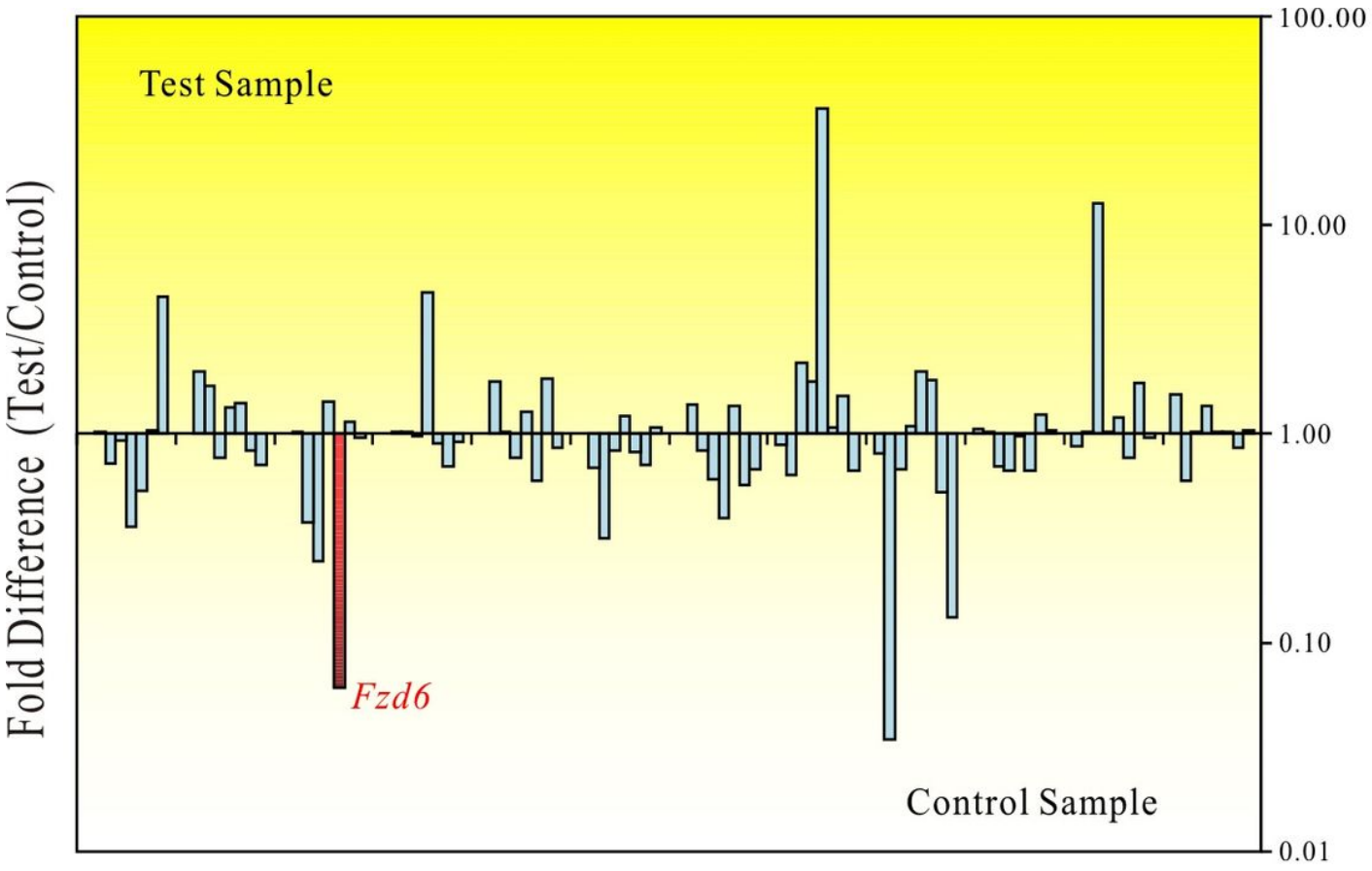

Figure 2

Gene chip results suggested that the expression of Fzd6 was decreased in OP-ASCs.

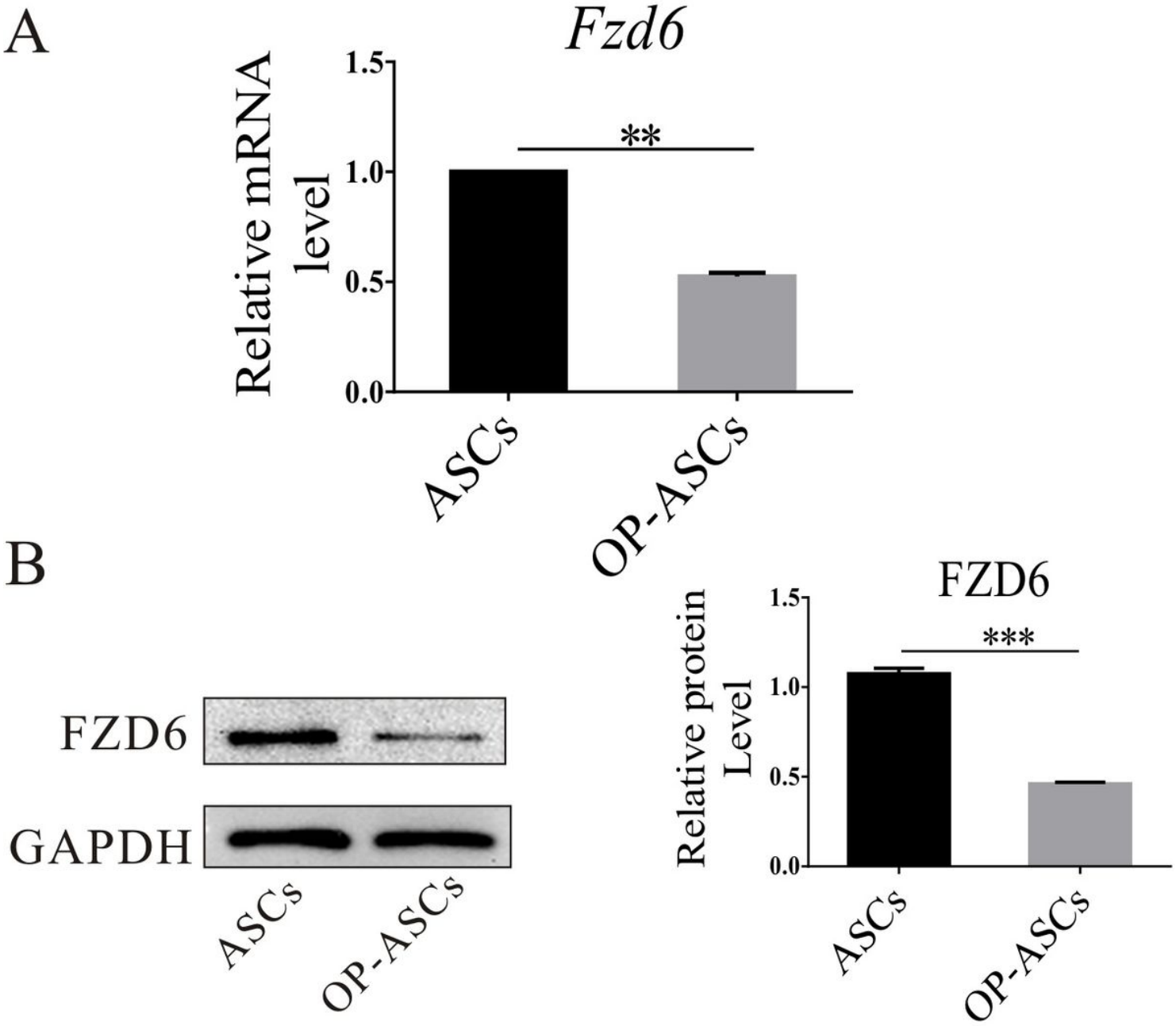

Figure 3

Gene and protein expression of Fzd6 in OP-ASCs. (A) Relative mRNA expression of Fzd6 in OP-ASCs. (B) FZD6 protein expression in OP-ASCs. (**P<0.01, ***P<0.001).

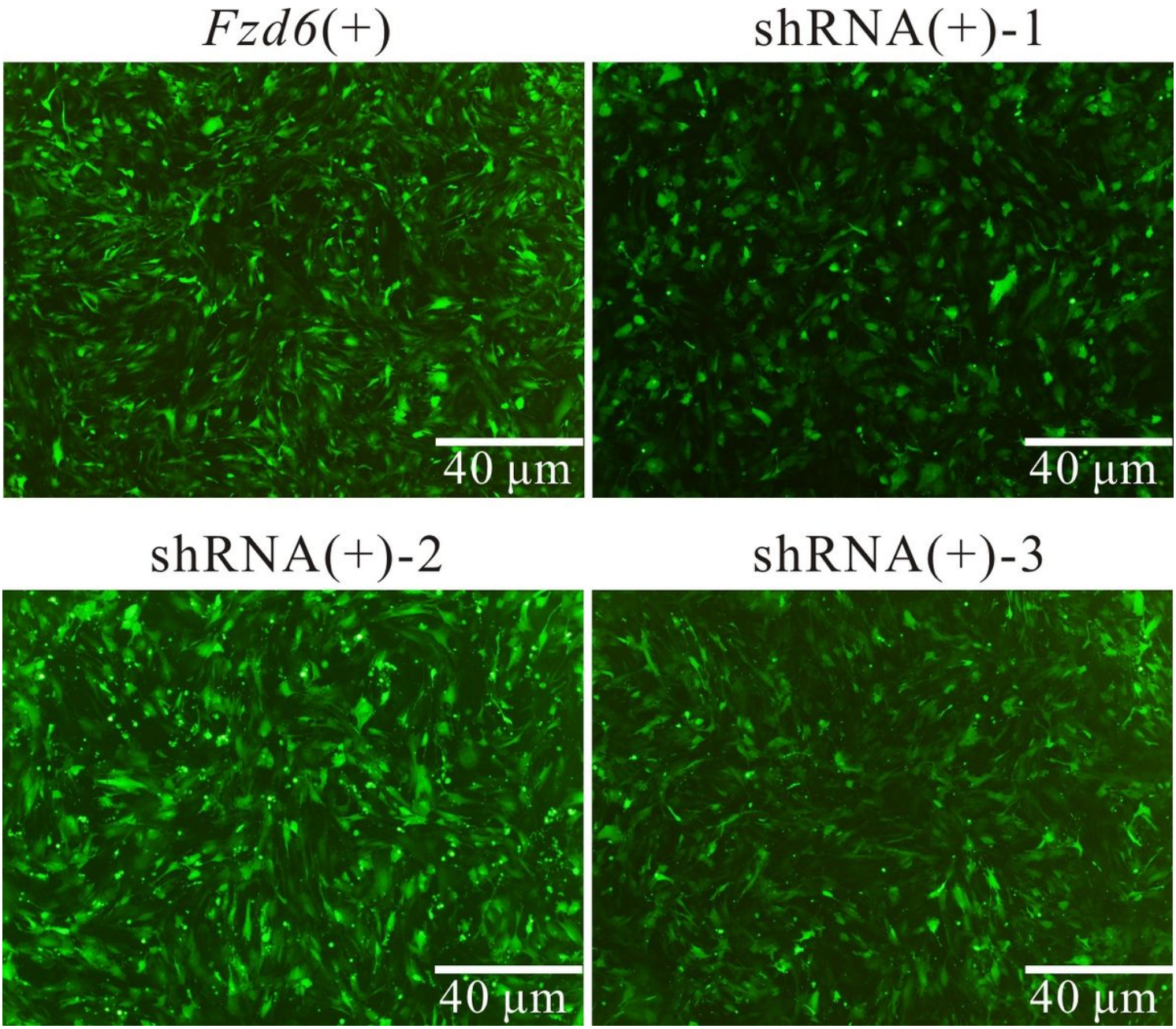

Figure 4

Fzd6 overexpression lentivirus and three Fzd6 silencing lentiviruses transfected into OP-ASCs with an MOI value of 80.

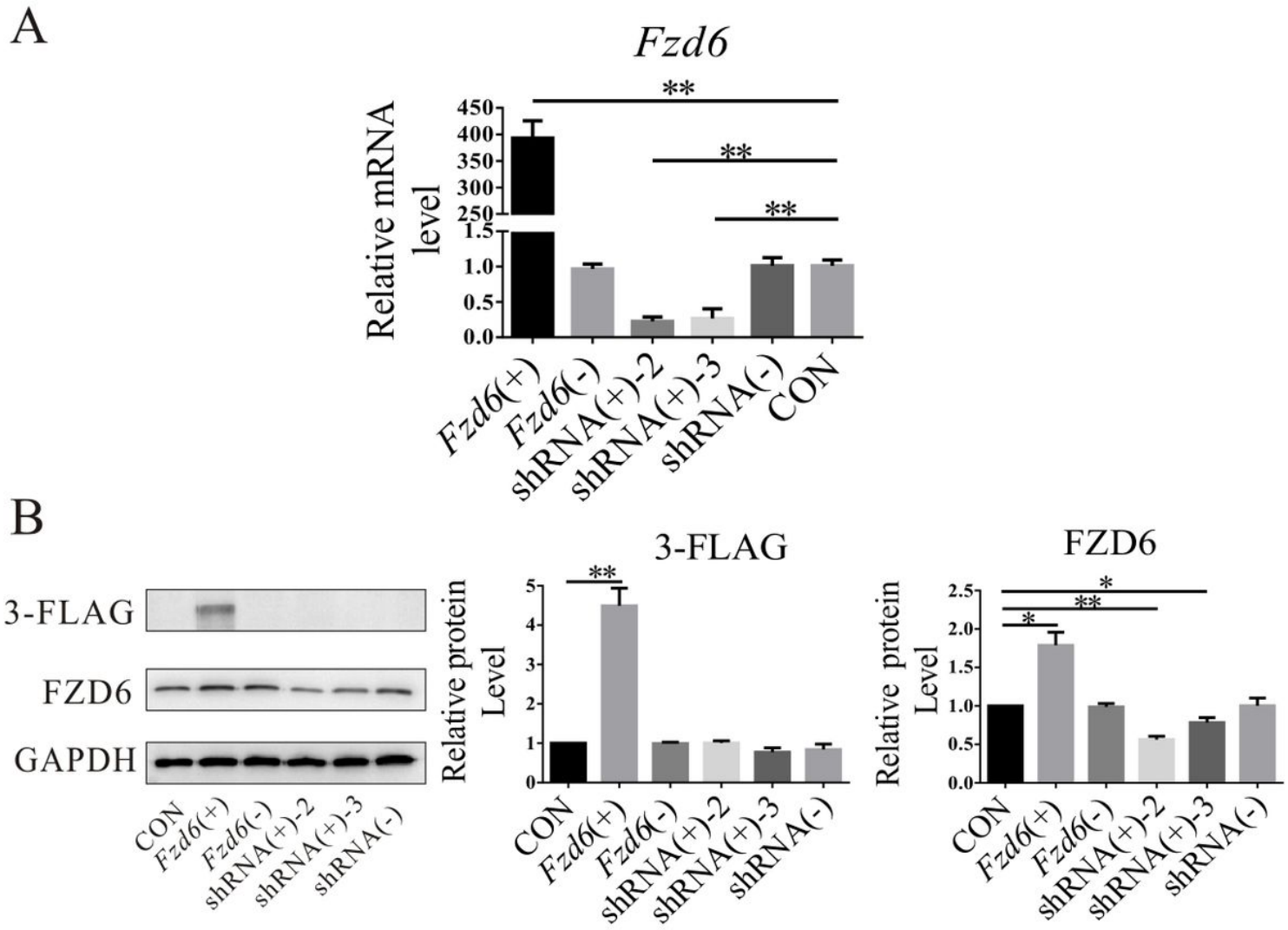

Figure 5

Overexpression or silencing Fzd6 lentivirus was transfected into OP-ASCs in vitro. (A) Relative mRNA expression of Fzd6 after lentivirus transfection in OP-ASCs. (B) Protein expression of 3-FLAG and FZD6 after lentivirus transfection in OP-ASCs. (*P<0.05, **P<0.01).

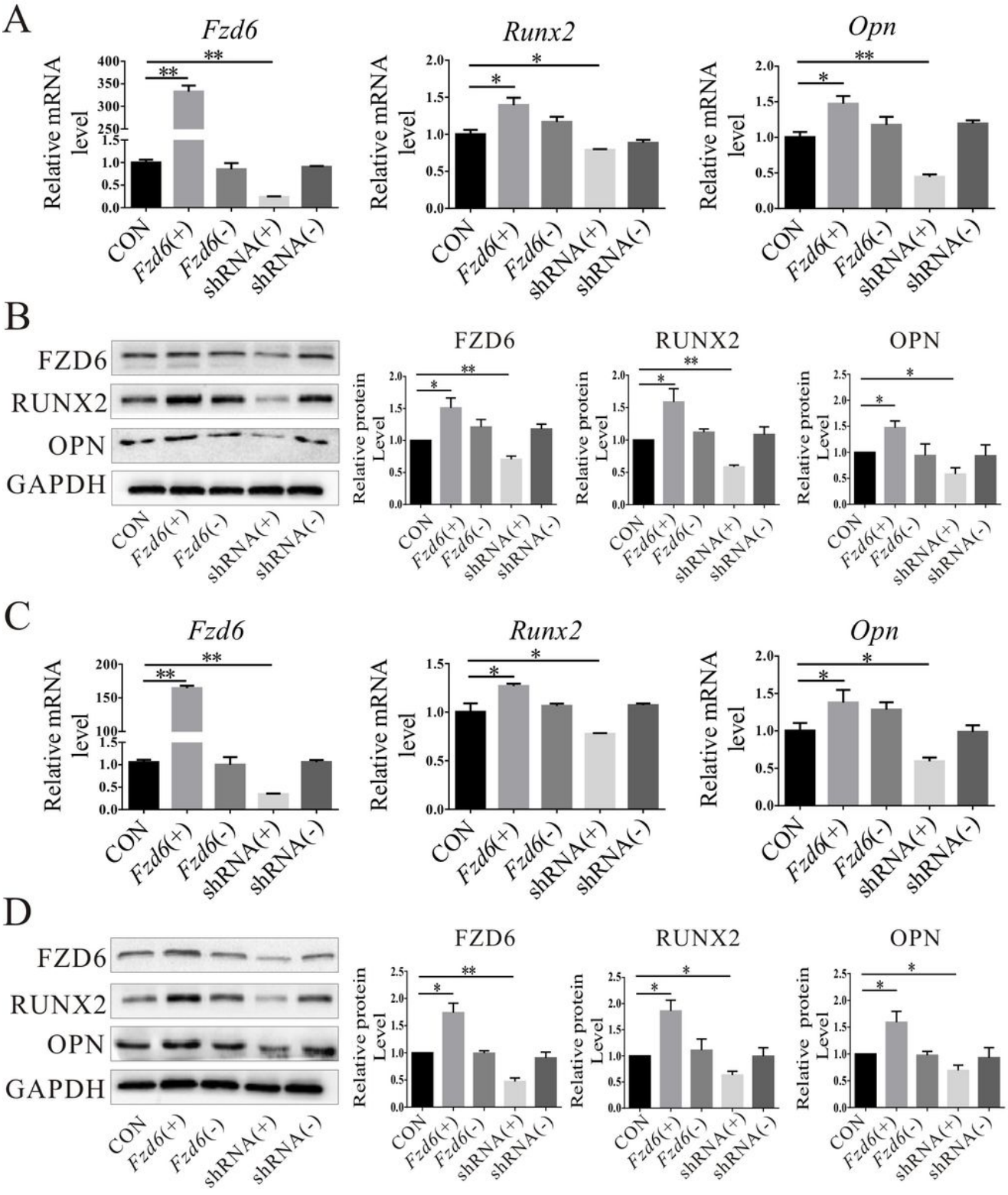

Figure 6

Osteogenic differentiation potential of OP-ASCs transfected with Fzd6 overexpression or silencing lentivirus in vitro. Relative mRNA expression of Fzd6, Runx2, and Opn after osteogenic induction for 3 d (A) and 5 d (C). Relative protein expression of FZD6, RUNX2, and OPN after osteogenic induction for 3 d (B) and 5 d (D). (*P<0.05, **P<0.01).

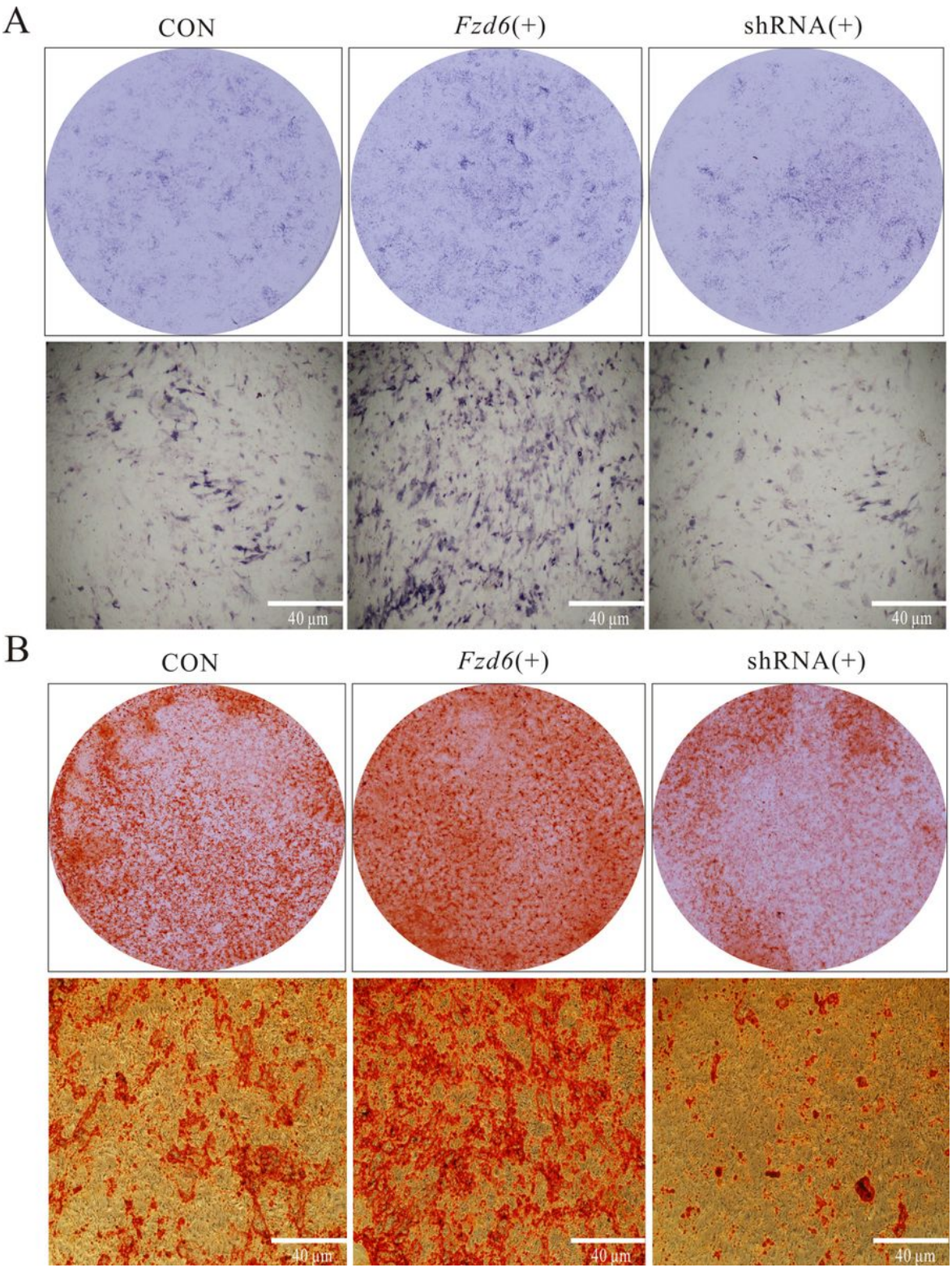

Figure 7

Osteogenic differentiation potential of OP-ASCs transfected with Fzd6 overexpression or silencing lentivirus in vitro. (A) ALP staining of OP-ASCs transfected with Fzd6 lentivirus after osteogenic induction for 7 d. (B) Alizarin red staining of OP-ASCs transfected with Fzd6 lentivirus after osteogenic induction for 14 d.

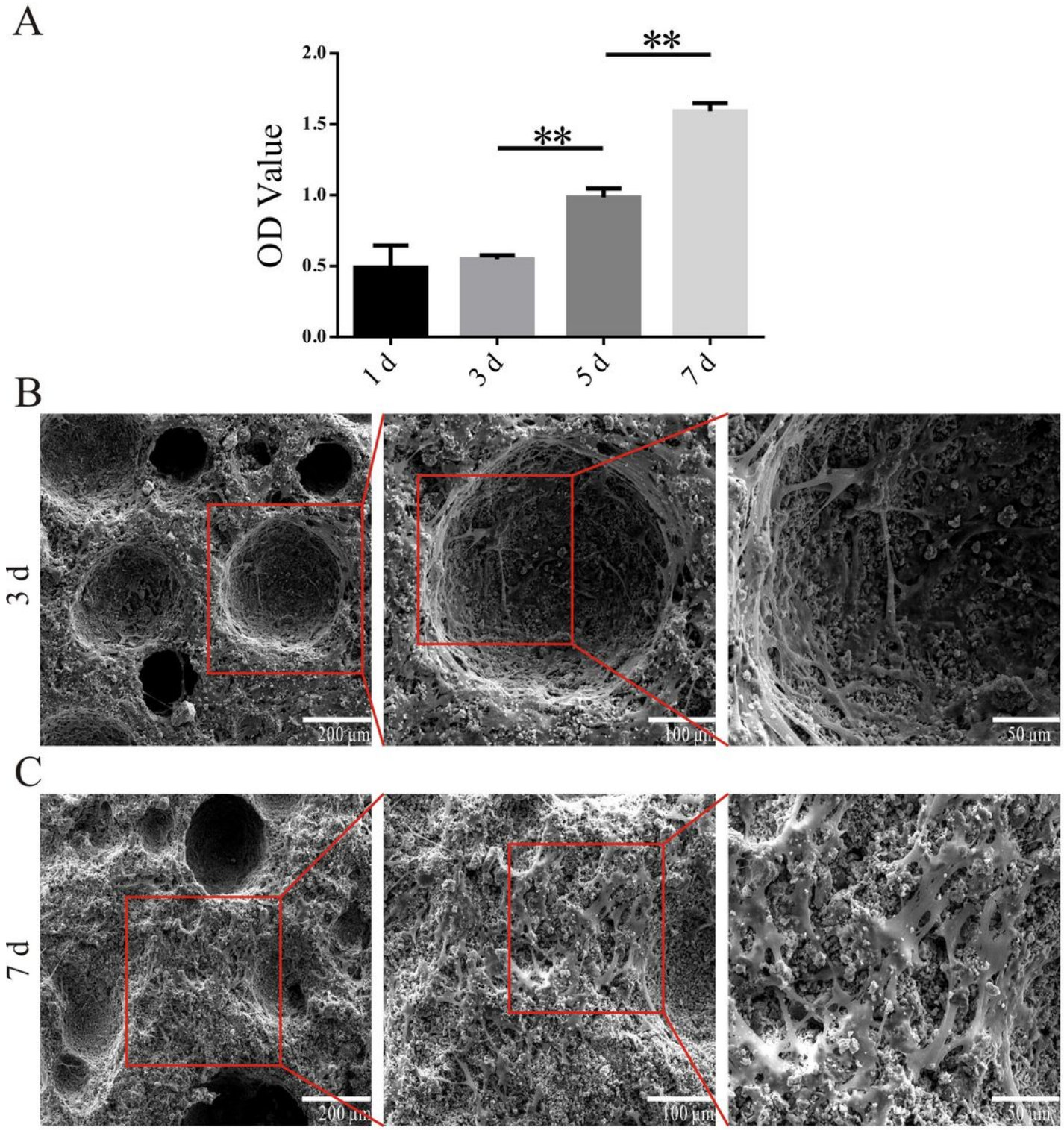

Figure 8

Osteogenic differentiation potential of OP-ASCs transfected with Fzd6 overexpression or silencing lentivirus in vivo. (A) Detection of cell proliferation at different times by CCK-8. (B, C) Scanning electron microscopy of OP-ASCs and BCP co-cultured for 3 d (B) and 7 d (C). (**P<0.01).

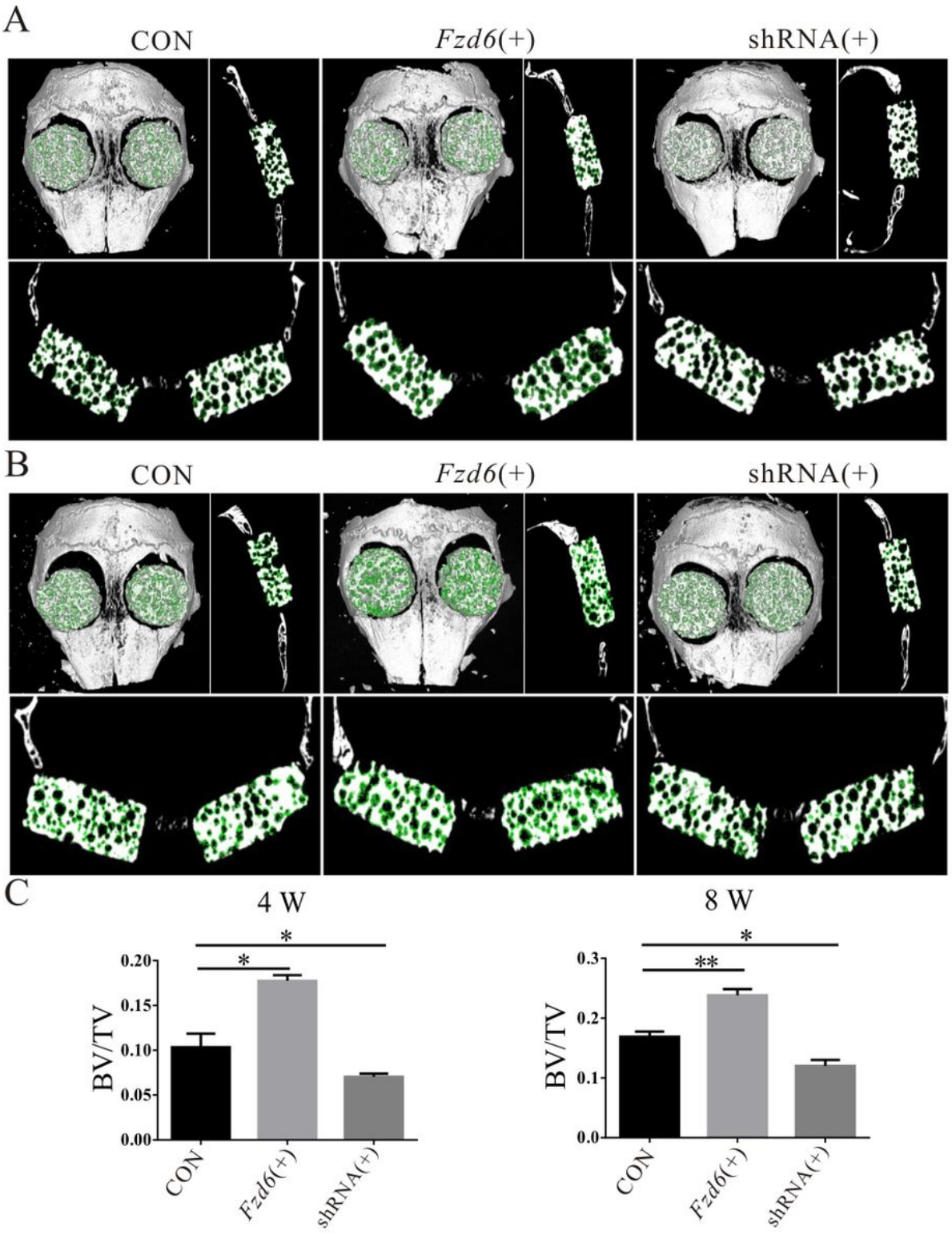

Figure 9

Osteogenic differentiation potential of OP-ASCs transfected with Fzd6 overexpression or silencing lentivirus in vivo. Micro-CT scan and three-dimensional reconstruction of mouse skull after transplantation of OP-ASCs for 4 w (A) and 8 w (B). (C) Coronal analysis, sagittal analysis, and BV/TV statistical analysis after transplantation of OP-ASCs for 4 w and 8 w (C). (*P<0.05,**P<0.01).

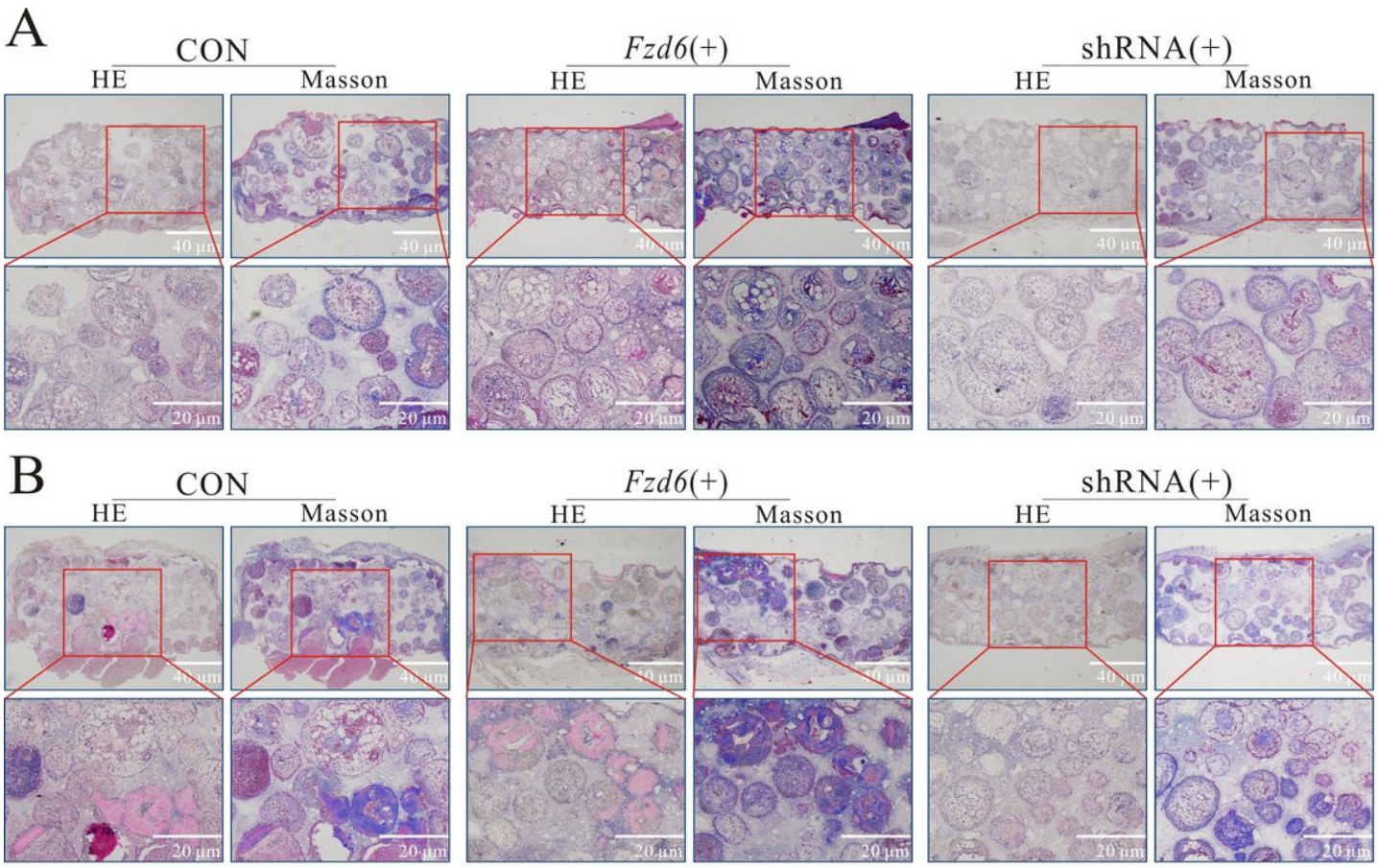

Figure 10

Osteogenic differentiation potential of OP-ASCs transfected with Fzd6 overexpression or silencing lentivirus in vivo. H&E and Masson staining of BCP after transplantation of OP-ASCs for 4 w (A) and 8 w (B).

Supplementary Files

This is a list of supplementary files associated with this preprint. Click to download.

- GraphicalAbstract.jpg